Peer-reviewed version available at *Polymers* **2017**, *9*, 509; doi:10.3390/polym9100509

Article

The Effect of Heat Transfer and Polymer Concentration on Non-Newtonian Fluid from Pore-Scale Simulation of Rock X-Ray micro-CT

Moussa Tembely , Ali M. AlSumaiti , Mohamed S. Jouini and Khurshed Rahimov

The Petroleum Institute, Abu Dhabi, UAE; mtembely@pi.ac.ae (M.T.); alsumaiti@pi.ac.ae (A.M.A); mjouini@pi.ac.ae (M.S.J.); krahimov@pi.ac.ae (K.R.)

* Correspondence: mtembely@pi.ac.ae;moussa.tembely@concordia.ca; Tel.: +971-2-607-5100

Abstract: Most of the pore-scale imaging and simulations of non-Newtonian fluid are based on the simplifying geometry of network modeling and overlook the fluid rheology and heat transfer. In the present paper, we developed a non-isothermal and non-Newtonian numerical model of the flow properties at pore-scale by direct simulation of the 3D micro-CT images using a Finite Volume Method (FVM). The numerical model is based on the resolution of the momentum and energy conservation equations. Owing to an adaptive meshing technique and appropriate boundary conditions, rock permeability and mobility are accurately computed. A temperature and concentration-dependent power-law viscosity model in line with the experimental measurement of the fluid rheology is adopted. The model is first applied at isothermal condition to 2 benchmark samples, namely Fontainebleau sandstone and Grosmont carbonate, and is found to be in good agreement with the Lattice Boltzmann method (LBM). Finally, at non-isothermal conditions, an effective mobility is introduced that enables to perform a numerical sensitivity study to fluid rheology, heat transfer, and operating conditions. While the mobility seems to evolve linearly with polymer concentration, the effect of the temperature seems negligible by comparison. However, a sharp contrast is found between carbonate and sandstone under the effect of a constant temperature gradient. Besides concerning the flow index and consistency factor, a good master curve is derived when normalizing the mobility for both the carbonate and the sandstone.

Keywords: pore-scale model; non-Newtonian fluid; Finite Volume Method; Digital Rock Physics

1. Introduction

Understanding reservoir rock and fluid properties is essential for applications such as oil and gas industry, water management, hydrology, and geosciences. Oil exploration and production in conjunction with the prospective impact on the environment is highly related to the fluid flowing inside the highly complex geometry of the porous media [1,2]. In order to optimize reservoir management, the fluid flow processes in porous media should be investigated through a multiscale approach ranging from the field to the core level, down to the pore scale. One of the most important petro-physical properties for reservoir rock is the permeability, a measure of the flow capacity of the pore network. It is function of the complex microstructure of the rock, fluid properties (density, viscosity) and parameters (velocity). Since no simple universal correlation exists for the permeability, an accurate and efficient numerical tool to predict the permeability is highly desirable [2–5].

Using the 3D micro-CT images, numerical simulation has been applied to perform the pore-scale imaging modelling ranging from (i) the widely used lattice Boltzmann method [6,7], (ii) the finite

difference method [5], (iii) finite element method [3], and more recently (iv) finite volume method approach [4]. Most of the numerical simulation concerns with the modeling at pore-scale deals with Newtonian fluid or simplified pore network, which significantly alters the porous media geometry, assuming it consists of connected capillary tubes [8,9]. Despite a large body of work, modeling of non-Newtonian is still challenging and remain an active field of research [8,10–12]. Furthermore, the effect of the temperature-dependent viscosity is still to be addressed at the pore scale. Predicting special core analysis (SCAL) data by means of digital rock physics (DRP) has gained attention recently. Most of the DRP simulations focus on Newtonian fluids and overlook the rheology of the fluid, which can be controlled by both the temperature and the polymer concentration. However, in petroleum engineering many fluids such as heavy oil and polymer solutions used for enhanced oil recovery (EOR) are non-Newtonian and non-isothermal at reservoir conditions. In order to use Digital Rock Physics (DRP) as a future tool to generating accurate, fast, and cost effective SCAL properties to support reservoir characterization and simulation; pore-scale modeling of non-Newtonian fluid at non-isothermal conditions is essential. This work proposes to shed a light on that aspect of the DRP.

In the present paper, we use a finite volume method (FVM) coupled with an adaptive meshing technique to perform the pore scale simulation from the micro-CT images of both a sandstone and a carbonate rocks from the literature. Besides, we performed simulations based on the LBM method for comparison and validation of the FVM on Newtonian fluid. Finally, we implement non-isothermal and non-Newtonian fluid models to test the pore-scale model sensitivity to both the rheological and operating parameters.

The paper is organized as follows: in Section 2, the governing equations are presented and in Section 3 the pore-scale modeling and validation are provided. Numerical results and sensitivity studies are performed in Section 4. Finally, conclusions are drawn in Section 5.

2. Pore-scale Governing equations

2.1. Mass and Momentum Conservations

The numerical simulation of a laminar flow inside a rock at pore-scale is considered. The fluid is assumed to be an incompressible non-Newtonian liquid. The continuity and momentum equations to be numerically solved in the finite volume method (FVM) formulation expresses as follows:

$$\nabla \cdot \mathbf{V} = 0 \tag{1}$$

$$\rho \mathbf{V} \nabla \mathbf{V} = -\nabla p + \rho \mathbf{g} + \nabla \cdot \tau \tag{2}$$

where $\mathbf{V}$ is the fluid velocity vector, and g denotes the gravity, while the fluid is assumed incompressible of density ρ. The stress tensor τ, assuming the viscosity depends on both the polymer concentration(C) and temperature (T), can be written function of the shear rate ($\dot{\gamma}$) as follows:

$$\tau = \mu(T, C, \dot{\gamma})[\nabla \mathbf{V} + \nabla \mathbf{V}^{\mathrm{T}}] \tag{3}$$

where μ is the viscosity which is assumed to be function to both concentration and temperature in addition to the dependency to the shear rate.

2.2. Energy conservation

In addition to the mass and momentum conservation, we solve the energy conservation equation, given below:

$$\rho C_p \nabla \cdot (\mathbf{V} T) = \nabla \cdot (\kappa T) + \phi_{Diss} \tag{4}$$

Preprints (www.preprints.org) | NOT PEER-REVIEWED | Posted: 15 September 2017 doi:10.20944/preprints201709.0059.v1

Peer-reviewed version available at Polymers 2017, 9, 509; doi:10.3390/polym9100509

where κ is the thermal conductivity and C_p is the heat capacity. In the energy conservation equation, we display the thermal viscous dissipation since fluid we are dealing with are generally non-Newtonian. The dissipation can be expressed as follows:

$$\phi_{Diss} = \tau : \nabla \mathbf{V} = \mu \left(\frac{\partial u_i}{\partial x_j} + \frac{\partial u_j}{\partial x_i} \right) \tag{5}$$

for simplicity we neglect the viscous dissipation since the Brinkman number, $Br = \mu U^2 / \kappa \Delta T \ll 1$, of the laminar flow withing the porous rock is small.

2.3. Temperature-Concentration Power-Law Viscosity Model

We propose for the viscosity a modified power-law accounting for the effect of the polymer concentration as follows:

$$\mu = \chi \exp \left[\alpha C - \beta (T - T_{ref}) \right] \dot{\gamma}^{n-1} \tag{6}$$

where C is the polymer concentration, T_{ref} the reference temperature α is a constant, χ is the consistency factor and n is the flow behavior index.

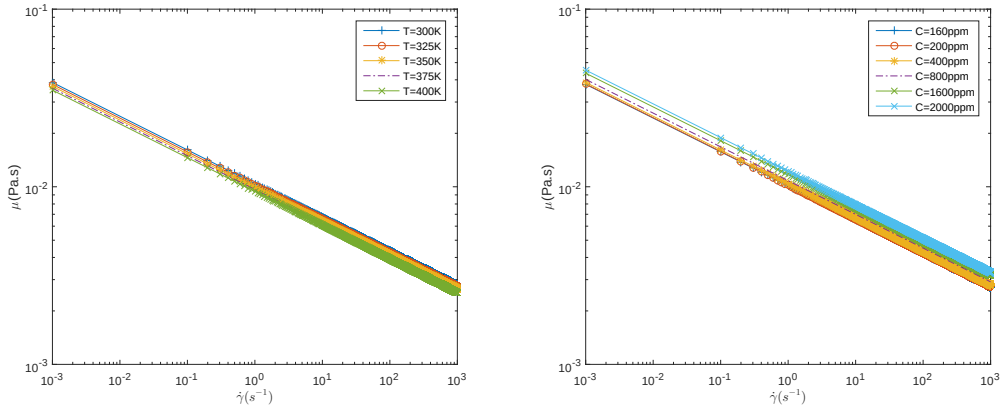

(a) (b)

Figure 1. Temperature-Concentration Dependent Power-Law Viscosity Fluid Function of the Shear Rate at Different (a) Concentrations and (b) Temperature from Eq.(6).

Table 1. Typical values of the viscosity model parameters

Parameters	χ	α	β	$Tref$	n
Values (SI)	10^{-2}	100	10^{-3}	293	0.81

The exponential dependency on the temperature can be explained by the Arrhenius type behavior. Eq. (6) can be used to simulate many polymer solutions of interest to the EOR, and the constants can be found through the experimental measurements of the fluid properties. Furthermore, the effect of polymer concentration on the shear thinning behavior of biopolymers such as Schizophyllan seems to be well-captured by the proposed model equation given in Eq. (6). This model (see Figure 1) is in line with experimental measurements of polymer solutions used for EOR [13]. Both the effect of temperature and concentration on the viscosity of polymer solutions are qualitatively well retrieved. The typical values used in Eq. (6) are given in Table 1. It is worth noting that even though our model may approximate well some polymers rheology for EOR, generally polymer solutions exhibit a more complex constitutive relations such as in the case of viscoelasticity.

Due to the challenge to perform experiments at the scale of the micro-CT 3D images resolution and the characterization of fluid flow within the pore network, the present work will be based on numerical simulations to gain insight into the physics of modeling complex fluid through a rock.

3. Numerical Approach and Validation

The workflow from the micro-CT image to the computation of petrophysical properties such as the permeability is summarized in Figure 2. The rock is first scanned at high resolution then segmented to discriminate between pore and solid phases; then the connectivity is determined in order to access the relevance of the numerical simulation. Finally the 3D digital rock model, the input of the numerical model, is generated.

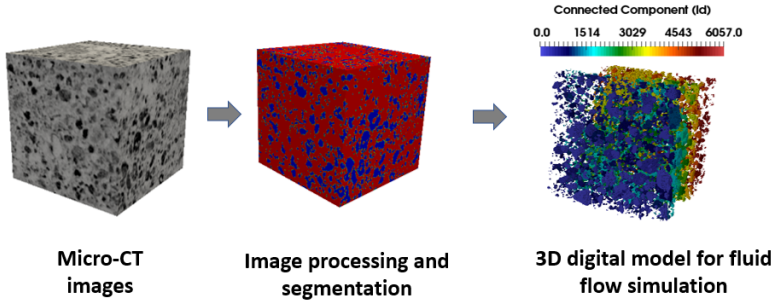

Figure 2. Workflow of the numerical simulation at pore-Scale of the micro-CT image of the rocks.

Before running the simulation, the segmented micro-CT image is meshed using SnappyHexMesh/C++ code by employing an adaptive meshing technique, through refinement and adjustment to fit onto the provided geometries of the rock. Besides incorporation of boundary layers' cells near the solid surface is also performed for better accuracy (Fig. 3).

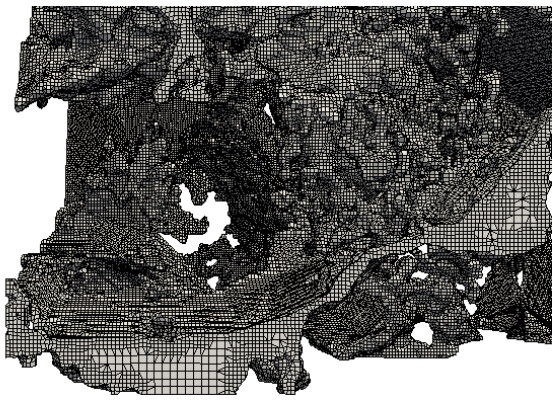

Figure 3. Pore-scale adaptive mesh from the digital image of the rock.

The pore-scale model is simulated by imposing a non-slip boundary conditions at the sides of the micro-plug sample and a pressure gradient between the inlet and outlet of the digital rock (Figure 4). After solving the fluid equation, the permeability can be computed following the general Darcy's law [14,15] as follows:

$$\Delta P = -\frac{\mu(T)}{A_o K_l} Q^{n-1} Q \tag{7}$$

where A_o is the outlet surface area of the sample and Q the flow rate computed by integration from the outlet as $Q = \int_{A_o} V dA$.

Preprints (www.preprints.org) | NOT PEER-REVIEWED | Posted: 15 September 2017 doi:10.20944/preprints201709.0059.v1

Peer-reviewed version available at Polymers 2017, 9, 509; doi:10.3390/polym9100509

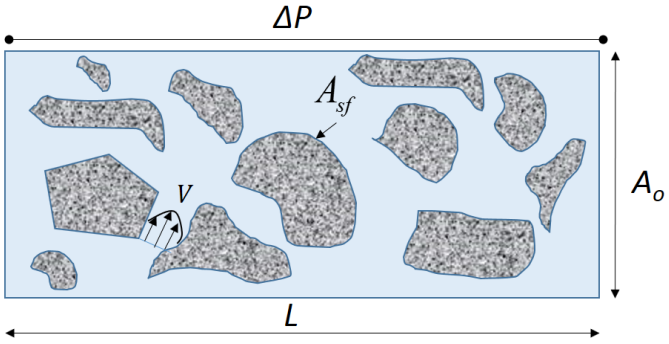

Figure 4. A schematic of the flow configuration at pore scale.

However, due to the non-Newtonian nature of the fluid and the dependency of the viscosity to both temperature and concentration, and for convenience, we will adopt an effective fluid mobility to characterize the non-Newtonian fluid flowing inside the porous media defined as:

$$M_{eff} = -\frac{1}{\Delta P}\frac{LQ}{A} \tag{8}$$

where Q is the flow rate, ΔP the pressure gradient imposed on the sample, L and A are the sample length and surface area, respectively. It accounts for all the relevant parameters for the non-Newtonian flow in the porous media, namely the porosity, temperature, concentration, intrinsic permeability. It's worth noting that for a Newtonian fluid, $n = 1$, the effective mobility reduce to $M_{eff} = k/\mu$. For comparison with experimental data, we will use the mobility in dimensionless form by scaled it by the mobility of the Newtonian fluid, in the present case water, $meff = M_{eff}/M_{effW}$.

The governing equations Eq. (1-6) are implemented in OpenFoam/C++. To solve the discretized equations within the FVM framework, a Semi-Implicit Method for Pressure-Linked Equations(SIMPLE) algorithm is used to calculate the pressure and velocity fields using a Generalized Geometric-Algebraic Multi-Grid (GAMG) solver in conjunction with a Gauss Seidel smoother. The convergence criteria set for the pressure and velocity fields is of the order of 10^{-6}. The simulation are performed on the two samples using the adaptive mesh technique consisting of 8368927 cells (8Million) and 15603561 cells (15Milions) for the Fontainebleau sandstone and the Grosmont carbonate, respectively. The simulations are run in parallel using a domain decomposition method.

3.1. Flow between two parallel plates

We first validate the model for a Poiseuille-Hagen flow with both a Newtonian and non-Newtonian fluids flowing between two parallel plates. The non-Newtonian fluid viscosity is taken as a power-law and is given below:

$$\mu(\dot{\gamma}) = K\dot{\gamma}^{n-1}, \tag{9}$$

for which an analytical solution can be written as:

$$V_x(y) = \frac{n}{n+1}\left(\frac{\Delta P}{KL}\right)^{1/n+1}\left[\left(\frac{h}{2}\right)^{1/n+1} - |\frac{h}{2} - y|^{1/n+1}\right] \tag{10}$$

or equivalently function of the flow rate Q,

$$V_x(y) = \frac{Q}{B(n,h)}\left[\left(\frac{h}{2}\right)^{1/n+1} - |\frac{h}{2} - y|^{1/n+1}\right] \tag{11}$$

Preprints (www.preprints.org) | NOT PEER-REVIEWED | Posted: 15 September 2017 doi:10.20944/preprints201709.0059.v1

Peer-reviewed version available at Polymers 2017, 9, 509; doi:10.3390/polym9100509

where $B(n,h) = 2(n+1)(h/2)^{2+1/n}/(2n+1)$. We performed the simulation at relatively low Reynolds number of, $Re = \rho V_0 D_0/\mu = 100$, to ensure a laminar flow.

The comparison between analytical and numerical solutions is provided in Fig. (5). A very good agreement of less than 0.5% the relative error is found.

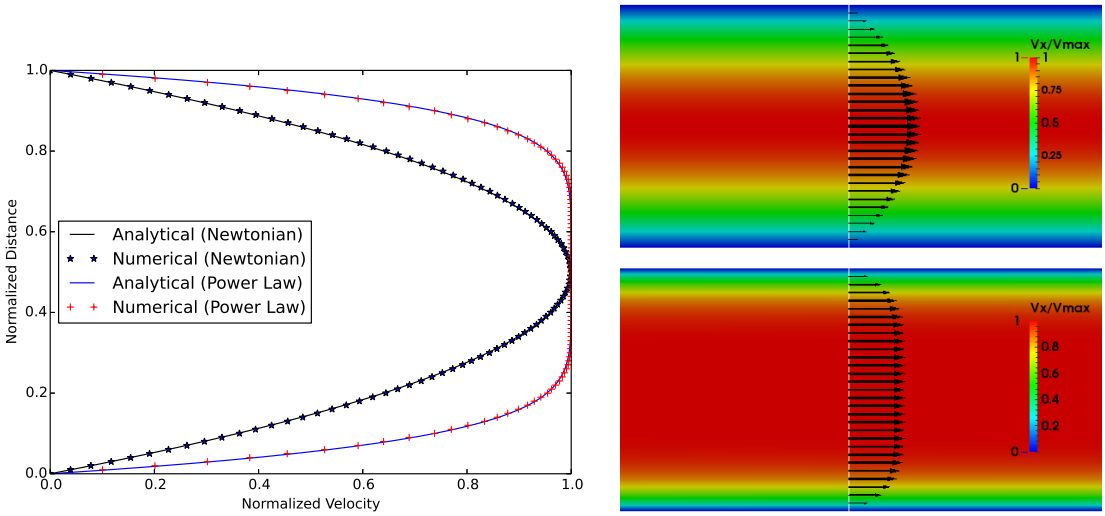

(a) Axial velocity profiles

(b) Axial velocity vector and contour for the Newtonian(top) and Non-Newtonian (bottom) cases

Figure 5. Comparison between numerical simulation and analytical solutions of the flow between two parallel plates, we set $K = 10^{-6}$ and $n = 0.2$ for the non-Newtonian fluid.

3.2. Flow in Porous Media

For validation purpose of our model in porous media, we apply the FVM model to 2 rocks samples from the literature, the Fontainebleau sandstone and Grosmont carbonate [3]. We performed the simulations under the same conditions using the widely used LBM (Palabos library) from the literature. We provide in Table 2 the simulation results (Figure 6) of the absolute permeability in (milliDarcy) along with the relative errors.

Table 2. Numerical Simulations Results of the Absolute Permeability in z-Axis

Sample	Image Size	Voxel Size (μm)	FVM	LBM	Relative Errors (%)
Fontainebleau Sandstone	288x288x300	7.5	1614	1610	0.2
Grosmont Carbonate	400x400x400	2.02	217	214	1.4

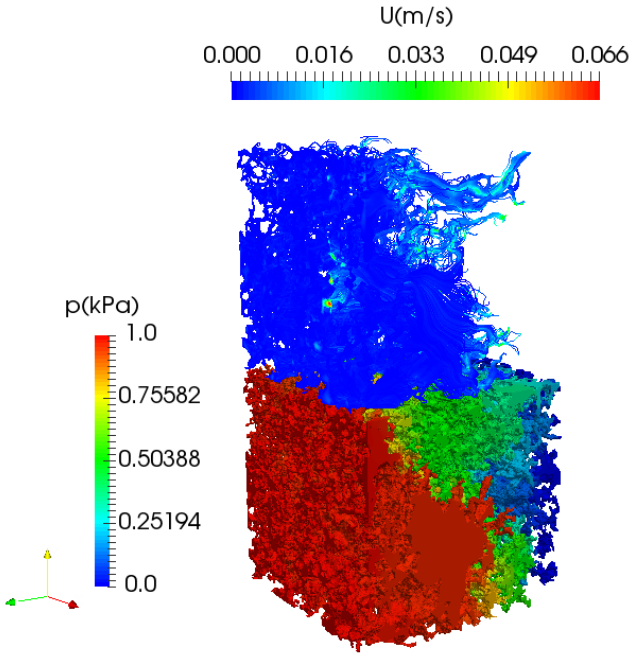

Figure 6. Simulated pressure field by FVM of the carbonate sample; streamlines are shown at the top of the pore structure for clarity.

The difference is less than 2% suggesting that the implemented finite volume method(FVM) is capable to simulate accurately at the pore-scale. Unlike in the LBM, extension of our FVM model to non-Newtonian fluid can be handled without any numerical tuning parameters.

4. Pore-scale Non-Newtonian and Non-isothermal Fluid Flow Simulation

4.1. Effect of the polymer concentration on the mobility

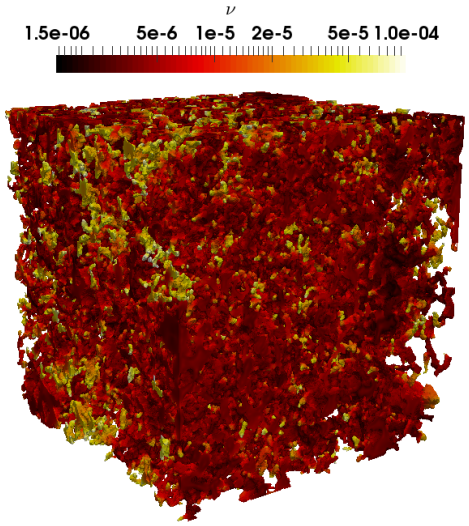

Figure 7. Simulated kinematic viscosity field $\nu(m^2/s)$ for the carbonate, displaying in logarithmic field for clarity.

In order to investigate the concentration effect, we simulated the fluid flow at pore-scale by varying the concentration at a fixed temperature using the proposed fluid rheology model given in Eq. (6). The kinematic viscosity field resulting from the simulation, which spans two orders of magnitude, is shown in Figure 7, highlighting the complexity nature of the concentration-dependent shear-thinning fluid flow within the rock. The effect of the concentration on the mobility for both the carbonate and sandstone are given in Figure 8. As expected, the mobility seems to evolve inversely proportional to the concentration. Interestingly, while the viscosity exponentially depends on the concentration, the mobility seems to evolve linearly with it for both samples.

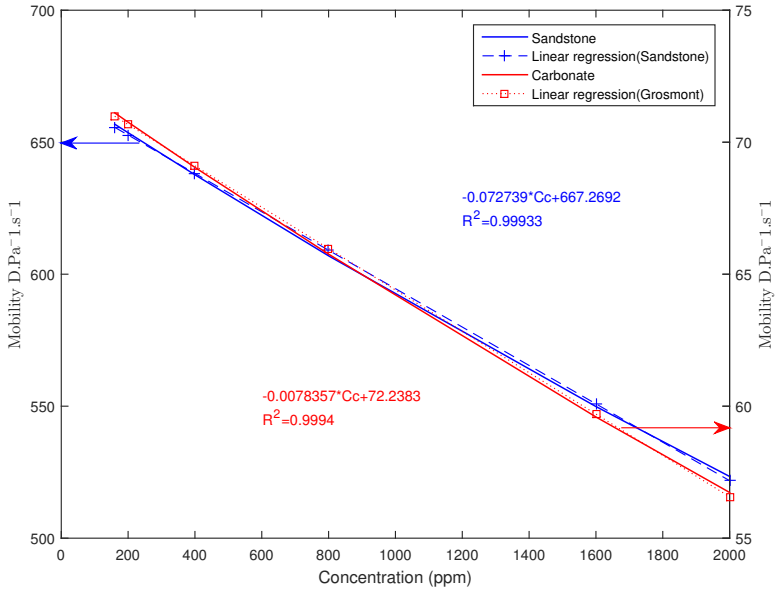

Figure 8. Simulated results of the variation of the effective mobility Eq. (8) function of the polymer Concentration.

4.2. *Effect of temperature gradient on the mobility*

We numerically impose different temperature gradients on the pore-scale model. The effect of temperature gradient seems to be very limited in controlling the mobility. However, an interesting evolution can be observed in Figure 9 highlighting the contrast between the two samples. Sandstone rock seems to follow a linear trend while the variation for the carbonate is non-monotonic. In fact, we can observe that the mobility dependency to the temperature gradient is complex, with trends difficult to predict. From the ambient condition an increasing of the temperature gradient leads to an increase of the mobility up until a point of inflexion where the mobility starts decreasing before bouncing back again at a much higher temperature gradient. This behavior seems to suggest that when dealing with non-Newtonian fluid in complex pore structured rock, such as carbonate, there may be an optimal temperature gradient to obtain higher mobility. A consequence of this finding may help in determining adequate operating conditions during oil production from wellbore where temperature gradient comes into play.

Preprints (www.preprints.org) | NOT PEER-REVIEWED | Posted: 15 September 2017 doi:10.20944/preprints201709.0059.v1

Peer-reviewed version available at Polymers 2017, 9, 509; doi:10.3390/polym9100509

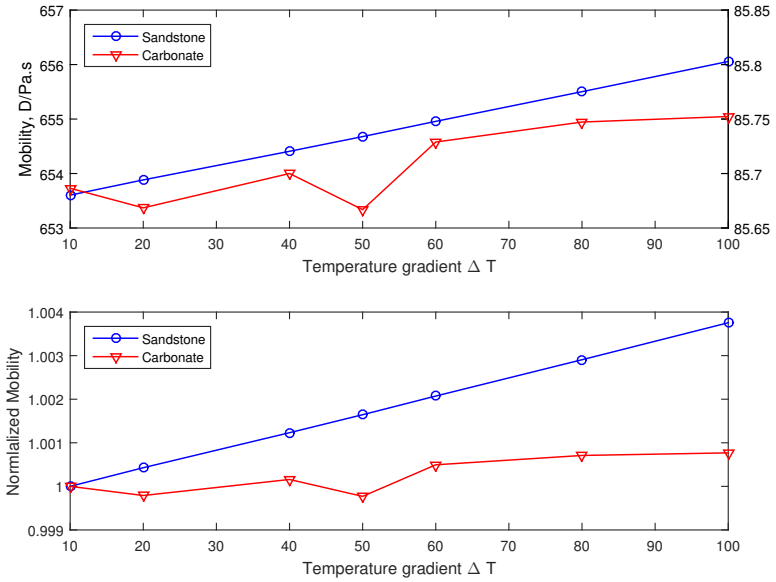

Figure 9. Variation of the effective mobility based on the temperature gradient imposed on the pore-scale model for the Fontainebleau sandstone and Grosmont carbonate.

4.3. Effect of the fluid rheological parameters on the mobility

We numerically investigate the sensitivity of the model to the rheological properties of the fluid, namely the flow behavior index n and the consistency factor K. We depict in Figure 10 the impact of both n and K on the mobility.

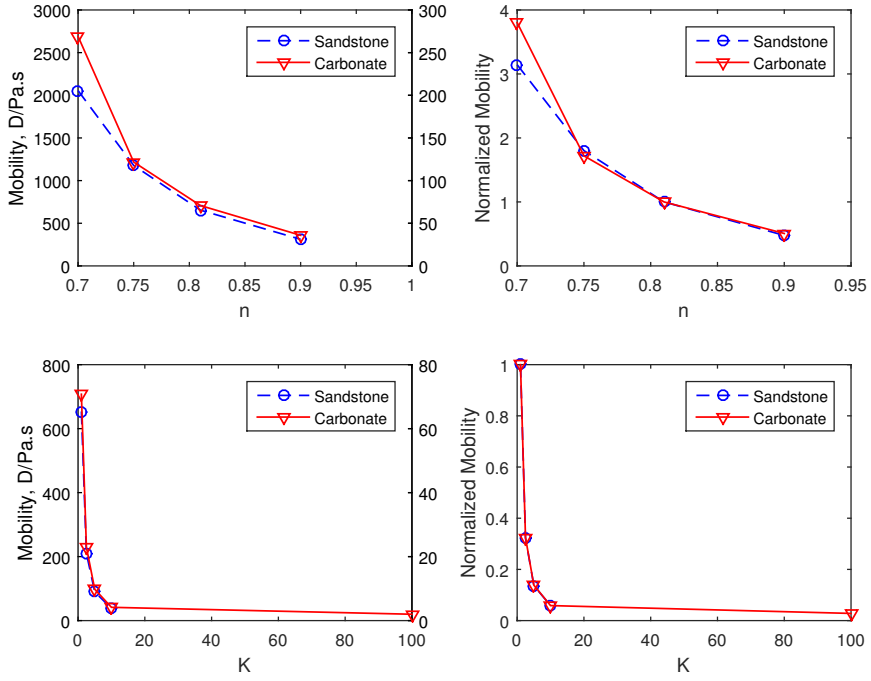

Figure 10. The sensitivity of the effective mobility to (top) the flow behavior index n and (bottom) the consistency factor (K) at a temperature of 300K and 200ppm of the polymer concentration. The effective mobility is being normalized with that of water as detailed in Section 2.

We observe that the mobility is reduced by an increase of both n and K. Even though, we have similar trends for both carbonate and sandstone on the fluid consistency factor(K), there is however

Preprints (www.preprints.org) | NOT PEER-REVIEWED | Posted: 15 September 2017 doi:10.20944/preprints201709.0059.v1

Peer-reviewed version available at Polymers 2017, 9, 509; doi:10.3390/polym9100509

a slight difference on the behavior index (n). In addition, the effect of K on the mobility seems to be more pronounced than that of n. It's worth noting the challenge posed experimentally to discriminate the effect of these two parameters contribution on the mobility. Hence, the possibility to perform such a sensitivity study numerically can help in the formulation of polymer solutions for EOR.

4.4. Effect of the pressure gradient

Here the model sensitivity under the effect of pressure gradient is investigated from the two samples, namely the Fontainebleau sandstone and the Grosmont carbonate. In Figure 11, we provide the simulation results where the evolution of the normalized flow rate and pressure gradient. We found that the results can be correlated to the following power-law, $Q/Q_{Newtonian} \approx \Delta P^{1/\xi}$. Interestingly, the parameter ξ evolves close to n, the flow behavior index, for the carbonate and $\xi = 1$ for the sandstone. The non-linearity nature of the fluid flow within the porous media seems to be more dominant for the carbonate, of complex structure, than for the sandstone sample. This effect is more pronounced at higher pressure gradient and ξ seems be a good parameter to reveal pore structure complexity.

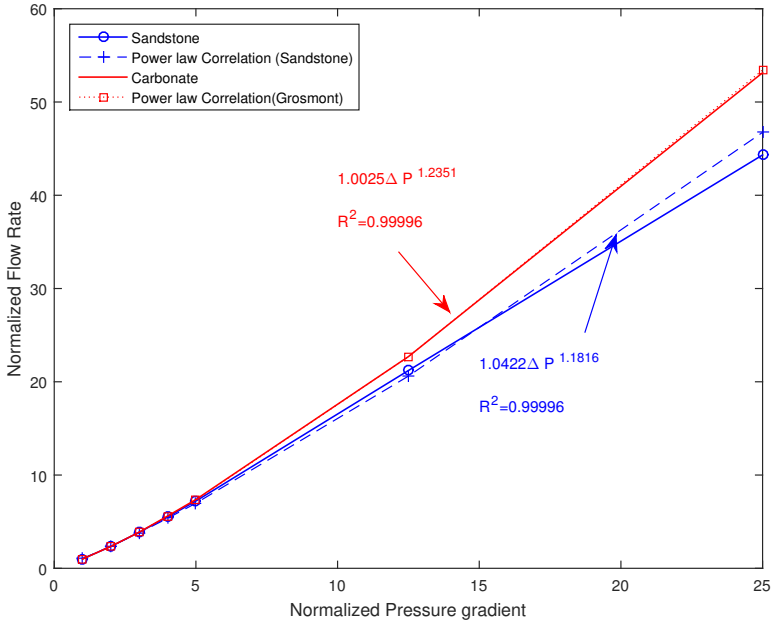

Figure 11. Simulated normalized flow rate and pressure gradient variation from pore-scale non-Newtonian model.

5. Conclusion

A comprehensive numerical model based on the Finite Volume Method (FVM) and an adaptive meshing technique to describe the flow properties at pore-scale of a non-Newtonian fluid is presented. The fluid rheology is modeled by incorporating its dependency to the concentration and temperature into a generalized power-law viscosity fluid model. Based on Newtonian fluid through rock samples from the literature, the FVM algorithm is validated against a Lattice Boltzmann Method (LBM). After implementing the non-Newtonian and non-isothermal fluids, the model is validated by simulating the fluid flow between two parallel plates for which the analytic solution is known. Subsequently, the model sensitivity to heat transfer and fluid rheology is tested by evaluating the effect of polymer concentration on the mobility as well as the relationship between flow rate and pressure gradient. The effective mobility dependency on the polymer concentration follows a linear trend while the flow rate displays a disparity between the carbonate and sandstone. Besides the fluid rheological properties such as the flow behavior index and consistency factor lead to a master curve when normalizing the mobility for both the carbonate and the sandstone. Overall, the present work serves to implement a

new simulator capable of computing the permeability and mobility of non-Newtonian fluid based on its thermal and rheological properties. The solver which can be used for different rock types at pore-scale can provide valuable insight into predicting flow behavior at reservoir conditions as well to better understanding polymer flooding for enhanced oil recovery (EOR).

Acknowledgments: Authors gratefully acknowledge the financial support from ADNOC and TOTAL under the Digital Rock Physics (DRP) project

Author Contributions: M.T., A.M.A., M.S.J. and K.R. designed the study; M.T. performed the study and wrote the paper. All the authors contribute to the paper.

Conflicts of Interest: The authors declare no conflict of interest.

References

1. Blunt, M.J.; Bijeljic, B.; Dong, H.; Gharbi, O.; Iglauer, S.; Mostaghimi, P.; Paluszny, A.; Pentland, C. Pore-scale imaging and modelling. *Advances in Water Resources* **2013**, *51*, 197 – 216. 35th Year Anniversary Issue.
2. Jouini, M.S.; Vega, S.; Al-Ratrout, A. Numerical estimation of carbonate rock properties using multiscale images. *Geophysical Prospecting* **2015**, *63*, 405–421.
3. Andrä, H.; Combaret, N.; Dvorkin, J.; Glatt, E.; Han, J.; Kabel, M.; Keehm, Y.; Krzikalla, F.; Lee, M.; Madonna, C.; Marsh, M.; Mukerji, T.; Saenger, E.; Sain, R.; Saxena, N.; Ricker, S.; Wiegmann, A.; Zhan, X. Digital rock physics benchmarks-part II: Computing effective properties. *Computers and Geosciences* **2013**, *50*, 33–43.
4. Guibert, R.; Nazarova, M.; Horgue, P.; Hamon, G.; Creux, P.; Debenest, G. Computational Permeability Determination from Pore-Scale Imaging: Sample Size, Mesh and Method Sensitivities. *Transport in Porous Media* **2015**, *107*, 641–656.
5. Mostaghimi, P.; Blunt, M.J.; Bijeljic, B. Computations of Absolute Permeability on Micro-CT Images. *Mathematical Geosciences* **2013**, *45*, 103–125.
6. Chen, S.; Doolen, G.D. Lattice Boltzmann method for fluid flows. *Annual Review of Fluid Mechanics* **1998**, *30*, 329–364, [https://doi.org/10.1146/annurev.fluid.30.1.329].
7. Wang, D.; Liu, Z.; Shen, J.; Liu, W. Lattice Boltzmann simulation of effective thermal conductivity of porous media with multiphase. *Journal of Porous Media* **2015**, *18*, 929–939.
8. Sochi, T. Non-Newtonian flow in porous media. *Polymer* **2010**, *51*, 5007 – 5023.
9. Fayed, H.E.; Sheikh, N.A.; Iliev, O. On Laminar Flow of Non-Newtonian Fluids in Porous Media. *Transport in Porous Media* **2016**, *111*, 253–264.
10. Tembely, M.; Vadillo, D.; Mackley, M.R.; Soucemarianadin, A. The matching of a "one-dimensional" numerical simulation and experiment results for low viscosity Newtonian and non-Newtonian fluids during fast filament stretching and subsequent break-up. *Journal of Rheology* **2012**, *56*, 159–183, [http://dx.doi.org/10.1122/1.3669647].
11. Avramenko, A.A.; Kuznetsov, A.V. Flow in a Curved Porous Channel with a Rectangular Cross Section. *Journal of Porous Media* **2008**, *11*, 241–246.
12. Gooneie, A.; Schuschnigg, S.; Holzer, C. A Review of Multiscale Computational Methods in Polymeric Materials. *Polymers* **2017**, *9*.
13. Quadri, S.M.R.; Shoaib, M.; AlSumaiti, A.M.; Alhassan, S. Screening of Polymers for EOR in High Temperature, High Salinity and Carbonate Reservoir Conditions. *International Petroleum Technology Conference* **2015**.
14. Di Federico, V.; Pinelli, M.; Ugarelli, R. Estimates of effective permeability for non-Newtonian fluid flow in randomly heterogeneous porous media. *Stochastic Environmental Research and Risk Assessment* **2010**, *24*, 1067–1076.
15. Pascal, H. Nonsteady flow of non-Newtonian fluids through a porous medium. *International Journal of Engineering Science* **1983**, *21*, 199 – 210.